Petroleum and Coal

Article   Open Access

Study the Fluid Loss and Rheological Behaviors of Bentonite Drilling Mud Contaminated with Salt and Used Motor Oil

Aram Mohammed Raheem

Civil Engineering Department, University of Kirkuk, Kirkuk, Iraq

Abstract

In this study, the fluid loss and rheological behaviors of 6% bentonite drilling mud contaminated individually with 6% salt and 6% used motor oil have been investigated. Two models represented by API static and kinetic fluid loss models have been used to examine the behavior of experimentally uncontaminated 6% bentonite drilling mud tested at room temperature and lasted for 120 minutes. In addition, both API and kinetic models were used to study the behavior of experimentally 6% bentonite drilling mud contaminated independently with 6% salt and 6% used motor oil tested under similar conditions as uncontaminated drilling mud. All the fluid loss tests have been performed under two different applied pressures represented by 25 psi (172 kPa) and 90 psi (621 kPa). Moreover, four different models represented by a power law, Bingham, Herschel- Buckley (H-B), and hyperbolic models were used to investigate the rheological behavior of experimentally uncontaminated 6% drilling mud tested under two different temperatures represented by 25ºC and 50ºC. The similar rheological study has been performed on experimentally 6% bentonite drilling mud contaminated separately with 6% salt and 6% used motor oil tested under similar conditions as uncontaminated drilling mud. For the applied pressure of 25 psi, it was shown that the maximum fluid loss is increased by 244% and 31% as the salt and used motor oil contaminations increased from 0% to 6% respectively. Furthermore, it was shown that the maximum shear stresses for 6% bentonite drilling mud tested at 50ºC increased by 104% and 59% as the salt and oil contaminations increased from 0% to 6% respectively. Finally, the kinetic model was better than API for fluid loss prediction and the hyperbolic model was the best for rheological properties evaluation with the highest R^2 of 0.98 and lowest RMSE of 0.14 Pa.

Keywords: fluid loss; rheological behavior; bentonite drilling mud; contamination; salt; used motor oil; kinetic model; API model; hyperbolic model; temperature; Bingham; power law; Herschel- Buckley.

1. Introduction

Boring mud or drilling fluid is a thick, viscous fluid combination that is used in oi and gas drilling progressions to carry rock cuttings to the surface and to lubricate and cool the drill bit [1]. In the drilling processes, the hydrostatic pressure prevents the collapse of unstable strata into the borehole and the infiltration of water from water-bearing strata that might be confronted [2]. The mud or drilling fluid system is the single constituent of the well-construction advancement that remains in contact with the wellbore during the entire drilling operation. The drilling-fluid systems are designed to exhibit severe wellbore conditions [3]. New enhancements in drilling-fluid expertise have made it attainable to reach a cost-effective, suitable-for-purpose system for every step in the well construction practice [4]. There are different types of drilling fluids based on their composition and uses. Three main factors affect the type of drilling fluid represented by the cost, technical implementation, and environmental influence. The annual classification of fluid schemes includes several categories of drilling fluids such as freshwater systems, saltwater system, oil or synthetic based systems, and pneumatic fluid system [5-6]. Oil based systems have been developed in the early 1960s to handle several drilling problems including clay swelling, the reaction between clay and formation, slough after exposure to

water based fluid systems, increasing downhole temperature, stuck pipe, contaminants, torque, and drag [7].

Commonly, saltwater drilling fluids are used for drilling salt formations and shale inhabitation [8]. This type of drilling fluids is established to restrain the formation to be similar as ice-type hydrates and accumulate around subsea wellheads and well-control equipment, blocking lines and impeding critical operations. The most used type of drilling mud is the water-based mud that is used frequently all around the world where the composition in mainly water and bentonite. The bentonite has the ability to add some degree of viscosity to the drilling mud and assists to carry drilled cuttings up the annulus of the well bore, and hence, it is being added to water based drilling mud [9].

In addition, clay or polymers can be added to generate the viscosity in the water based drilling mud. The clay is the cheapest and most broadly used additive for viscosity control in the water-based mud [10]. In the drilling mud, the clay is responsible for intensifying viscosity to enhance the lifting capacity of the mud to transport cuttings to the surface, especially in larger holes where annular velocity is low. Furthermore, the clay can facilitate to build a wall filter cake in permeable zones to prevent fluid loss [11].

The contamination in the drilling mud is extremely a serious problem that can happen during drilling operation [12]. Mud can be contaminated when any foreign material appears the mud system and produces unfavorable changes in the mud properties such as the viscosity, the density, and filtration. Water based mud systems are highly exposed to contamination among other kinds of drilling muds. Mud contamination can be caused by over treating the mud system with additives or from the material entering into the mud during drilling. The most frequent contaminants of water-based drilling mud systems are solids gypsum/anhydrite, makeup water, soluble sulfides, cement/lime, salt / saltwater flow, and soluble bicarbonates and carbonates.

The most affected characteristics are the rheological properties including yield stress, plastic viscosity, filter cake, and gel strength, stability against contamination, and stability under different operating conditions [13]. A number of factors can affect the rheological properties of the drilling mud such as pressure, temperature, and contaminants [14]. In the drilling operations, the drilling mud is polluted with different contaminants such as salts, cement, and drill solids. Salt contamination can come from salt beds during drilling or from formation water influx. At high temperature, the drilling mud remedy is required since the mud is unable to tolerate the contaminants [15]. The drilling fluid efficiency and performance in drilling operation is influenced by its rheological properties, so it is required to investigate the drilling mud rheological properties and parameters at the downhole conditions [16].

The rheological properties of two drilling muds have been studied, and the results have shown that the drilling mud with stable properties is needed at high pressures and temperatures [13]. The effect of NaCl salt as a contaminant on the rheological properties of bentonite drilling mud has been studied where both plastic viscosity and electrical resistivity were decreased with increasing salt content [17]. It was shown that the contamination could increase the filter loss by 30% and decrease the electrical resistivity by 86% compared to the same sample with no contamination [18]. The effect of different electrolyses on the viscosity of water based drilling mud at different testing conditions has been investigated [19]. This study has concluded that NaCl salt contamination increases the shear stress versus shear strain rate relationship whereas KCl contamination decreases the shear stress versus shear strain rate relationship of water based drilling mud. The effect of polyelectrolyte in salt-free and salt contaminated drilling fluid systems have been examined [14]. The polyelectrolyte is a super fluid loss reducer and might be used as a stabilizer for bentonite drilling mud by building good temperature resistance with anti-aging performance. The effects of pressure and temperature on the drilling mud properties have been studied by many researchers [20-21]. In addition, the effect of salt contamination on the drilling fluid has been examined by some researchers [22].

The main objective of this study is to investigate the effects of salt and used motor oil contaminations on the behavior of bentonite drilling mud. The specific objectives are as follows:

1. Study the effect of salt and used motor oil contaminations on the fluid loss behavior of 6% bentonite drilling mud tested at room temperature under the effect of two applied pressures represented by 25 psi (172 kPa) and 90 psi (621 kPa) and all the tests lasted for 120 minutes. In addition, API and kinetic models were used to predict the fluid loss behavior.
2. Examine the effect of salt and used motor oil contaminations on the rheological behavior of 6% bentonite drilling mud tested under two different temperatures represented by 25° C and 50° C. Moreover; power law, Bingham, Herschel- Buckley (H-B), and hyperbolic models were used to evaluate the rheological behavior.

2. Materials and methods

2.1. Material

2.1.1. Bentonite

The mineral bentonite is found all around the world. It is the result of volcanic ash weathering. Bentonite has the ability to react as a fluid when mechanically stressed especially when it is shaken or stirred. Nevertheless, it hardens in inactive condition due to the viscosity increase. In this study, unaltered light commercial sodium bentonite was used to prepare water based drilling mud with 6% bentonite (w/w) content. The hydraulic conductivity of the bentonite was $1*10^{-9}$ m/sec.

2.1.2. Salt

Sodium chloride or salt is an ionic compound with a chemical formula of NaCl representing a 1:1 ratio of sodium and chloride ions. Sodium chloride is the responsible for the salinity of seawater, and it is generally used as a condiment and food preservative.

2.1.3. Used motor oil

Crude oil or petroleum (in this study "heavy used engine oil"), is unprocessed oil found deep beneath the surface of the earth. Its color ranges from clear to black and found as a liquid or solid. The overall properties of the crude oils are dependent upon their chemical compositions and structure. The crude oil consists of hydrocarbons compounds. The main hydrocarbons exist in crude oil are aliphatics, alicyclics and Polycyclic Aromatic Hydrocarbons (PAH).

2.2. Methods

2.2.1. OFITE model 900 viscometer

The OFITE model 900 viscometer is a small portable fully automated system used for measuring fluid viscosity. It is made of cylindrical rotational viscometer, which uses a transducer to determine the induced angle of rotation of the bob by a fluid sample. The tested fluid is contained in the shear gab or annular space between the rotor and bob, which is connected to a shaft with a spring.

The viscous drag generated by the fluid produces a torque on the bob that is observed by the transducer that computes the angular displacement of the bob.

2.2.2. Filter press

The series 300 LPLT filter press (API Filter Press) is the most used means for measuring the filtration properties of the drilling muds and cement slurries. LPLT filter press assemblies contain a mud reservoir mounted in a frame, pressure source, filtering medium, and a graduated cylinder for collecting filtrate. As specified by the American Petroleum Institute (API), the working pressure is 100 psi (689 kPa), and the filtering area is 7.1 in^2 (46 cm^2). The filter press design features a cell body to hold the mud sample, a pressure inlet, and a base

cap with screen and filter press. These units have been used by the industry for field and laboratory uses.

2.2.3. Drilling mud mixer

Drilling fluid formulations are normally mixed using different shearing devices having either fixed or variable speeds. API recommends single mud impeller blade where the blades can be in different forms such as rounded propellers, waveform shapes, and sharp blades. These mixers can also be used to mix cement for laboratory or field-testing

3. Modeling

3.1. Modeling of the rheological properties

3.1.1. Power law

The power law model is a fluid model that used to define a non-Newtonian fluid where there an exponential relationship between shear stress and shear strain rate as follows:

$$\tau = K_1\gamma^{n_1} \tag{1}$$

where: K_1 = is the fluid consistency unit; n_1 = is the power law exponent.

$$\frac{d\tau}{d\gamma} = K_1 n_1 \gamma^{n_1-1} \tag{2}$$

$$\frac{d^2\tau}{d\gamma^2} = (n_1-1)n_1 K_1\gamma^{n_1-2} \tag{3}$$

When $\gamma = \infty \Rightarrow \tau_{max} = \infty \tag{4}$

Thus, the upper shear stress limit condition is not satisfied when power law model is used.

3.1.2. Bingham model

Bingham model is a two-parameter rheological model that is widely used to describe the flow characteristics of many types of drilling muds. The mathematical form of the model is as follows:

$$\tau = Y_p + P_v * \gamma \tag{5}$$

where: τ= shear stress, γ = shear rate, Y_P = yield point, P_V = plastic viscosity.

Fluid obeys the Bingham model exhibit a linear shear stress-shear strain rate behavior. The plastic viscosity (P_V) clearly identifies the slope of the line, and the yield point (Y_P) is the threshold shear stress. P_V is kept as low as possible for fast drilling to minimize colloidal solids. Y_P should be high enough to transport cuttings out of the hole, but not so large as to create extreme pump pressure as the mudflow starts. Y_P is controlled using different choices of mud treatment.

3.1.3. Herschel–Bulkley model (H-B model)

The Herschel–Bulkley model is defined a fluid using three parameters that can be represented mathematically as follows [24]:

$$\tau = \tau_{o2} - K_2\dot{\gamma}^{n_2} \tag{6}$$

where τ, τ_{o2}, γ, K_2 and n_2 represent the shear stress (Pa), yield stress (Pa), shear strain rate (1/s), correction parameter and flow behavior index respectively.

For the rigid material; the model assumes that below the yield stress (τ_o), the slurry behaves as a rigid solid similar to Bingham plastic model. For the material flows as a Power law fluid, the exponent n describes the shear thinning and shear thickening behavior. Slurries are considered as shear thinning when n<1 and shear thickening when n>1. A fluid becomes shear thinning when the apparent viscosity decreases with the increase in shear strain rate.

Thus, the model should satisfy the following conditions:

$$\frac{d\tau}{d\dot{\gamma}} = K_2 n_2\dot{\gamma}^{(n_2-1)} > 0 \Rightarrow K_2 n_2 > 0 \tag{7}$$

$$\frac{d^2\tau}{d\gamma^2} = K_2 n_2(n_2-1)\dot{\gamma}^{(n_2-2)} \Rightarrow K_2 n_2(n_2-1) < 0$$

when $\dot{\gamma} \to \infty \Rightarrow \tau_{max} = \infty$ (8)

Hence, Herschel–Bulkley model does not satisfy the upper limit condition for the shear stress limit.

3.1.4. Hyperbolic model

Relationship between shear stress and shear strain rate of water based drilling mud was inspected. Based on the investigation of the laboratory tested data, the following hyperbolic relationship can be proposed:

$$\tau - \tau_0 = \frac{A}{A + D\dot{\gamma}}$$ (9)

where τ_0 is the yield stress (Pa), $A(\text{Pa s})^{-1}$, and $D(\text{Pa})^{-1}$, are model parameters and $\dot{\gamma}$ is the shear strain rate (s^{-1}).

$$\frac{d\tau}{d\dot{\gamma}} = \frac{(A + D\dot{\gamma})(0) - AD}{(A + D\dot{\gamma})^2} = \frac{-AD}{(A + D\dot{\gamma})^2} > 0 \Rightarrow A > 0$$

$$\frac{d^2\tau}{d\dot{\gamma}^2} = \frac{-2AD^2}{(A + D\dot{\gamma})^3} < 0 \Rightarrow D > 0$$

when $\dot{\gamma} = \infty \Rightarrow \tau_{max} = \frac{1}{D} + \tau_0$ (10)

It is clearly shown that this model has a limit on the maximum shear stress, which can be produced by the fluid at a relatively high rate of shear strains.

3.2. Modeling of the filtering process

3.2.1. General model

The traditional method to calculate the infiltration through filter cake is given by the following equations [25-26]. The filter press is used to determine: (1) the filtration rate in a standard filter paper, and (2) the rate of mud cake thickness increase on the standard filter paper. Based on Darcy's law, the rate of infiltration is given by:

$$\frac{dv_f}{dt} = \frac{k(t)A_o\Delta P}{\mu(T)h_{mc}} > 0$$ (11)

During the filtration process, the volume of infiltrated solids in the mud is equal to the volume of deposited solids in the filter cake:

$$f_{sm}(t)V_m = f_{sc}(t)h_{mc}A_o$$ (12)

where f_{sm} = volume fraction of solids in the mud and f_{sc} = volume fraction of solids in the cake.

$$f_{sm}(t)(h_{mc}A_o + V_f) = f_{sc}(t)h_{mc}A_o$$ (13)

$$h_{mc} = \frac{f_{sm}(t)V_f}{A_o(f_{sc}(t) - f_{sm}(t))} = \frac{V_f}{A_o\left(\frac{f_{sc}}{f_{sm}}(t) - 1\right)}$$ (14)

Substituting Eq. (14) into Eq. (11):

$$\int_0^{V_f} V_f dV_f = \int_0^t \frac{k(t)A_o\Delta P}{\mu(T)} A_o\left(\frac{f_{sc}}{f_{sm}}(t) - 1\right)dt$$ (15)

3.2.2. Static model (API model)

The static model has been build based on the following assumptions:
1. It was assumed that the filter cake is formed initially; however, this is not true since at the start there is no cake formation in either experimental or real field situation.
2. The percentage of solids in the cake to the solids in the mud is constant, but in fact, it increases with time to a limiting value when the flow is stopped.
3. The cake permeability is constant, but in reality, it should decrease with the time.

By applying these assumptions to equation (15) and performing the integration with the initial condition, the following equation is obtained:

$$V_f - V_0 = \sqrt{2k\Delta P\left(\frac{f_{sc}}{f_{sm}} - 1\right)}A_0\frac{\sqrt{t}}{\sqrt{\mu}}$$ (16)

Equation (16) can be re-written as follows:

$$v_f - v_0 = M * \sqrt{t}$$ (17)

where: V_f = volume of fluid loss (cm^3), v_0 = initial volume of fluid loss (cm^3), k = drilling mud permeability (Darcy), k_0 = initial permeability of drilling mud (Darcy), ΔP = applied pressure (atm), f_{sc} = Volume fraction of solid in the cake, f_{sm} = volume fraction in mud, V_m = volume of solids in mud, A_0 = filter is a (cm^2), t = time (minute), μ = mud viscosity (cp), h_{mc} = the thickness of the filter mud cake (cm), $M = \sqrt{\frac{2k\Delta P\left(\frac{f_{sc}}{f_{sm}}-1\right)}{\mu}}A_0$.

If the time is considered to be (∞) in Eq. (17), the volume of the fluid loss will be (∞), and this cannot happen in reality. Hence, static (API) model does not satisfy the total filtration volume.

3.2.3. New kinetic (hyperbolic) model

This model is developed based on the fact that the rate of infiltration is dependent on several factors such as the permeability of the filter cake, the ratio of the solid content in the cake to the solid content in the mud, and the time [27].

$$\frac{dv}{dt} = f\left(k(t), \frac{f_{sc}}{f_{sm}}(t)\right) = Nk^L\left(\frac{f_{sc}}{f_{sm}}\right)^p \tag{18}$$

This model has the following features:
1. The rate of change in the permeability can be quantified as shown in Eq. 19 with L=1:

$$k = \frac{2A_1 * k_\circ}{(A_1 + B_1 t)^2} \tag{19}$$

2. The ratio of the solid content in the cake to the solid content in the mud as a volume fraction is a function of time shown in Eq. 20 with p=1:

$$\left(\frac{f_{sc}}{f_{sm}} - 1\right) = \frac{\alpha_\circ t}{A_1 + B_1 t} \tag{20}$$

3. The final form of the filtration equation exhibits the form of hyperbolic function after substituting Eqs. (19) and (20) into Eq. (15) and performing integration of the equation with applying the initial conditions:

$$V_f - V_0 = N * \frac{t}{A_1 + B_1 t} \tag{21}$$

where: A_1 = fluid loss parameter, B_1 = arbitrary constant (1/min), α_0 = arbitrary constant (1/min), A_0 = filter area (cm^2), V_0 = Initial value of drilling mud infiltration (cm^3),

$N = \sqrt{\frac{2 * k_0 * \alpha_0 * \Delta P}{\mu(T)}} * A_o$.

The parameter A_1 represents the initial rate of the infiltration, while the constant B_1 represents the final stage of infiltration. Moreover, Eq. (21) satisfies the following criteria:
1. The total infiltration volume has a limiting value where no more infiltration could happen because the particle is blocking all the open porous in the filter cake medium.
2. None of the mentioned properties can be checked in the API model; however, these changes in the properties can be monitored in the field or the laboratory. In addition, this model can be used to model both short and long term infiltration-time relationships.
3. Both A_1 and B_1 are functions of pressure and time.

3.3. Comparison of model predictions

In order to evaluate the accuracy of any model predictions in the study, both the root mean square error (RMSE) and the coefficient of determination (R^2) as defined in Eqs. (22) and (23) were quantified using [28]:

$$RMSE = \sqrt{\frac{\sum_{i=1}^{n}(y_i - x_i)^2}{N_2}} \tag{22}$$

$$R^2 = \left(\frac{\sum_i (x_i - \bar{x})(y_i - \bar{y})}{\sqrt{\sum_i (x_i - \bar{x})^2}\sqrt{\sum_i (y_i - \bar{y})^2}}\right)^2 \tag{23}$$

where y_i is the actual value; x_i is the calculated value from the model; $\bar{y}$ is the mean of actual values; $\bar{x}$ is the mean of calculated values and N_2 is the number of data points.

4. Results and analysis

4.1. General

The results and analysis of 28 laboratory experimental tests conducted on water based drilling mud where 14 experiments have done to model the filtration phenomenon and the rest have been performed for the rheological properties. For the fluid loss experiments, two set of tests have been performed using pressures of 25 psi and 90 psi on 6% uncontaminated bentonite drilling mud and the tests have lasted for 120 minutes. The same fluid loss experimental tests have been done on 6% bentonite drilling mud contaminated separately with salt and used motor oil using pressures of 25 psi and 90 psi and the tests have lasted for 120 minutes. For the rheological experiments, two set of tests have been performed at two different temperatures at 25°C and 50°C on 6% uncontaminated bentonite drilling mud. Similar rheological experimental tests have been performed on 6% bentonite drilling mud contaminated individually with salt and used motor oil at two different temperatures at 25°C and 50°C.

4.2. Filtration experimental tests

The validity of both kinetic hyperbolic and API models was considered for long-term results (t > 30 min). Most of the real laboratory or field tests can be performed for more than 30 min; therefore, it is important to check the filtration phenomenon for more than 30 min where implicit changes occur in cake permeability, so the lid content ratio in the cake to the mud, and cake porosity.

The variation of fluid loss with time for uncontaminated 6% bentonite drilling mud under two different applied pressures of 25 psi and 90 psi have shown in Fig. 1. The experimental tests have done at room temperature and lasted for 120 minutes. With increasing the time, the API model prediction increased with no limit on the fluid loss compared to the kinetic hyperbolic model that limited the maximum fluid loss to (V_o + N/B). The effect of applied pressure is ignored in the API model whereas both A and B parameters include the effect of applied pressure in the kinetic hyperbolic model. Experimental tests have shown that the maximum fluid loss for the 6% bentonite drilling mud at the final tested time of 120 min were 35 cm³ and 42 cm³ at applied pressures of 90 psi and 25 psi respectively. As the applied pressure increased from 25 psi to 90 psi, the maximum fluid loss increased by 20% because fluid flow increased under the effect of higher applied pressure.
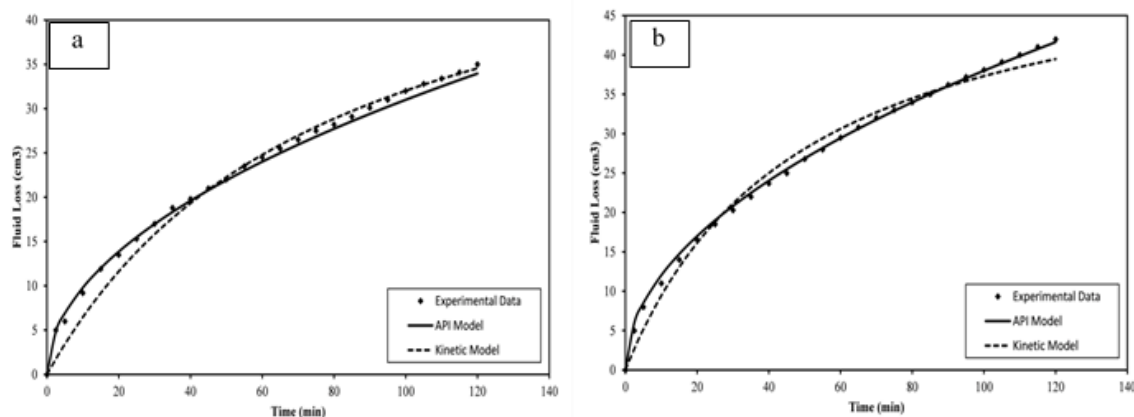

Figure 1. The variation of fluid loss with time for uncontaminated 6% bentonite drilling mud at room temperature under two different applied pressures of (a) applied pressure = 25 psi, and (b) applied pressure = 90 psi

Similarly, the variation of fluid loss with time for 6% bentonite drilling mud contaminated with 6% salt under two different applied pressures of 25 psi and 90 psi have shown in Fig. 2. The experimental tests have done at room temperature and lasted for 120 minutes. Experimental tests have shown that the maximum fluid loss for the 6% bentonite drilling mud contaminated with 6% salt at the final tested time of 120 min was 120.5 cm³ and 132.8 cm³ at

applied pressures of 90 psi and 25 psi respectively. As the applied pressure increased from 25 psi to 90 psi, the maximum fluid loss increased by 10% because fluid flow increased under the effect of higher applied pressure. For the applied pressure of 25 psi, the maximum fluid loss is increased by 244% as the salt contamination increased from 0% to 6%. For the applied pressure of 90 psi, the maximum fluid loss is increased by 216% as the salt contamination increased from 0% to 6%. The salt has the tendency to increase the fluid loss since the salt increases the flocculation of clay particles that leads to more particles settlement in a shorter time.
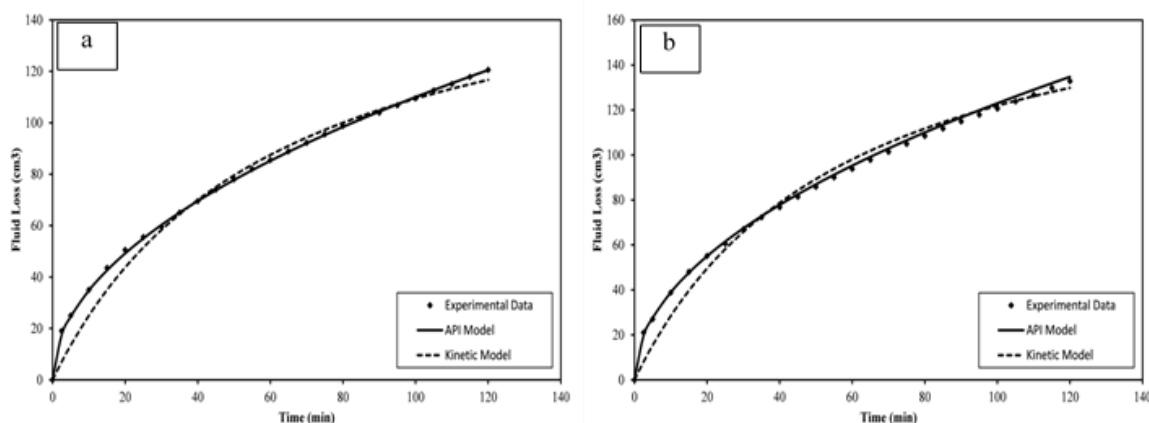

Figure 2. The variation of fluid loss with time for 6% bentonite drilling mud contaminated with 6% salt at room temperature under two different applied pressures of (a) applied pressure = 25 psi, and (b) applied pressure = 90 psi

Similarly, the variation of fluid loss with time for 6% bentonite drilling mud contaminated with 6% used motor oil under two different applied pressures of 25 psi and 90 psi have shown in Fig. 3.
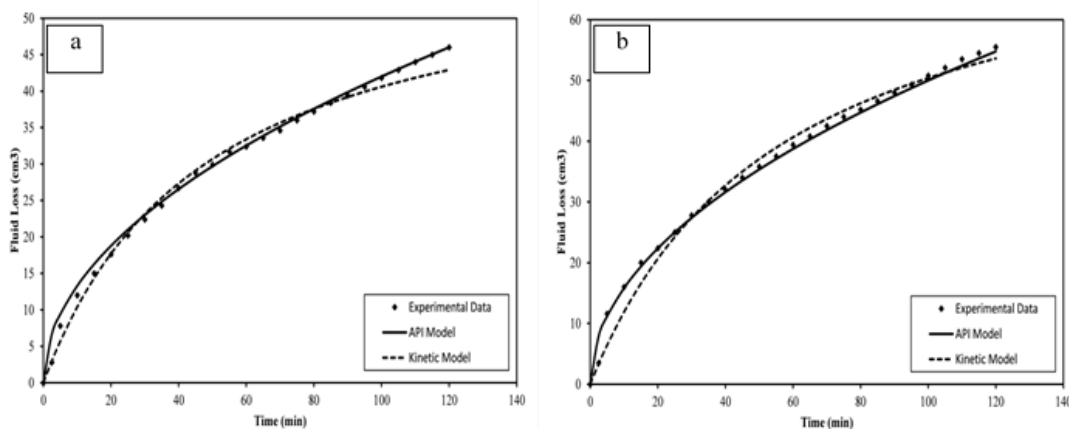

Figure 3. The variation of fluid loss with time for 6% bentonite drilling mud contaminated with 6% used motor oil at room temperature under two different applied pressures of (a) applied pressure = 25 psi, and (b) applied pressure = 90 psi

The experimental tests have done at room temperature and lasted for 120 minutes. Experimental tests have shown that the maximum fluid loss for the 6% bentonite drilling mud contaminated with 6% used motor oil at the final tested time of 120 min were 46 cm^3 and 55.5 cm^3 at applied pressures of 90 psi and 25 psi respectively. As the applied pressure increased from 25 psi to 90 psi, the maximum fluid loss increased by 21% because fluid flow increased under the effect of higher applied pressure. For the applied pressure of 25 psi, the maximum fluid loss is increased by 31% as the used oil contamination increased from 0% to 6%. For the applied pressure of 90 psi, the maximum fluid loss is increased by 32% as the used oil contamination increased from 0% to 6%. The oil has the tendency to increase the fluid loss

since the oil decreases the friction between the clay particles that leads to more particles settlement in a shorter time.

4.3. Rheological properties analysis

The rheological experimental tests have been performed on uncontaminated 6% bentonite drilling mud under two different temperatures of 25°C and 50°C. In addition, similar experimental tests have been performed on 6% bentonite drilling mud contaminated separately with 6% salt and 6% used motor oil.

4.4. Experimental tests at 25°C

The variation of shear stress with a shear strain rate of uncontaminated 6% bentonite drilling mud at 25°C has shown in Fig. 4. Four different models including power law, Bingham, Herschel-Buckley (H-B), and Hyperbolic models have been used. All the model parameters with their accuracy predictions have summarized in Table 1. The maximum measured shear stress for uncontaminated 6% bentonite drilling mud at 25°C was 8.6 Pa at a shear strain rate of 1700 (1/s). All the models predicted the maximum shear stress very well with the highest R^2 of 0.97 and lowest RMSE of 0.3 Pa.

Table 1. Models prediction parameters for uncontaminated 6% bentonite drilling mud tested at 25°C

Bentonite (%)	Salt (%)	Oil (%)	τ_0 (Pa)	K	n	RMSE (Pa)	R^2	τ_0 (Pa)	μ (cP)	RMSE (Pa)	R^2
				Power law					**Bingham**		
6	0	0	1.9	0.8	0.62	0.46	0.93	2.1	0.0035	0.3	0.97

Bentonite (%)	Salt (%)	Oil (%)	τ_0 (Pa)	k (Pa.s)	n	RMSE (Pa)	R^2	τ_0 (Pa)	A (Pa^{-1})	B (Pa)$^{-1}$	RMSE (Pa)	R^2
				Herschel- Buckley (H-B)					**Hyperbolic**			
6	0	0	1.79	0.06	0.66	0.35	0.93	2.5	255	0.008	0.3	0.97

The variation of shear stress with a shear strain rate of 6% bentonite drilling mud contaminated with 6% salt at 25° C has shown in Fig. 5. Four different models including power law, Bingham, Herschel-Buckley (H-B), and Hyperbolic models have been used. All the model parameters with their accuracy predictions have summarized in Table 2. The maximum measured shear stress for 6% bentonite drilling mud contaminated with 6% salt at 25°C was 5.8 Pa at a shear strain rate of 1700 (1/s). All the models predicted the maximum shear stress very well, and the hyperbolic model was the best with the highest R^2 of 0.98 and lowest RMSE of 0.14 Pa. The maximum shear stress for 6% bentonite drilling mud tested at 25° C decreased by 48% as the salt contamination increased from 0% to 6% because the salt causes dispersion between clay particles leads to lower measured maximum shear stress.

Table 2. Models prediction parameters for 6% bentonite drilling mud contaminated with 6% salt tested at 25°C

Bentonite (%)	Salt (%)	Oil (%)	τ_0 (Pa)	K	n	RMSE (Pa)	R^2	τ_0 (Pa)	μ (cP)	RMSE (Pa)	R^2
				Power law					**Bingham**		
6	6	0	1.4	0.06	0.62	0.3	0.93	1.8	0.0027	0.18	0.97

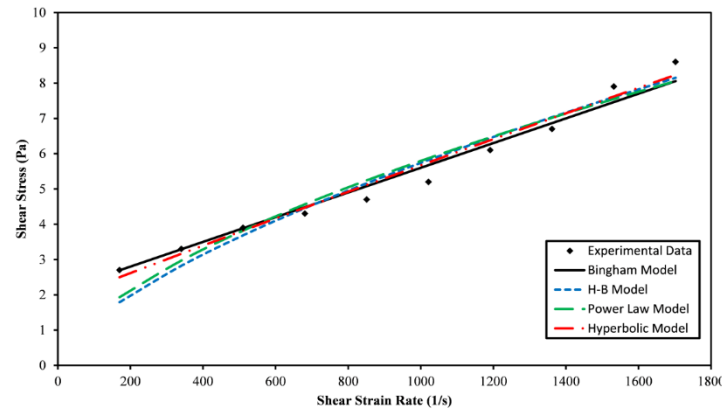| Bentonite (%)	Salt (%)	Oil (%)	τ_0 (Pa)	k (Pa.s)	n	RMSE (Pa)	R^2	τ_0 (Pa)	A (Pa^{-1})	B (Pa)$^{-1}$	RMSE (Pa)	R^2
				Herschel- Buckley (H-B)					**Hyperbolic**			
6	6	0	1.8	0.055	0.62	0.3	0.93	2	380	0.008	0.14	0.98

Figure 4. The variation of shear stress with shear strain rate for uncontaminated 6% bentonite drilling mud tested at 25°C
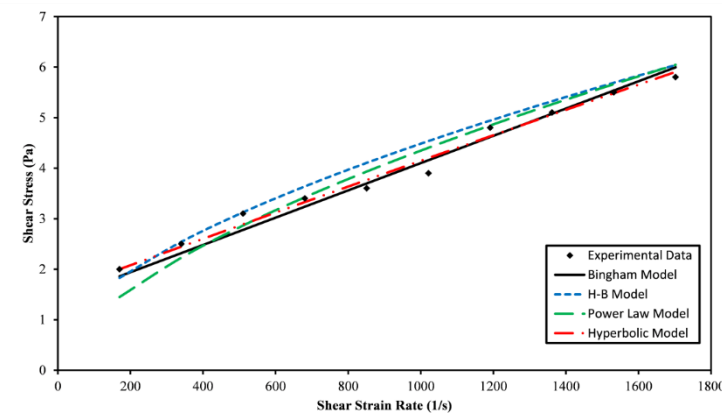

Figure 5. The variation of shear stress with shear strain rate for 6% bentonite drilling mud contaminated with 6% salt tested at 25°C

The variation of shear stress with a shear strain rate of 6% bentonite drilling mud contaminated with 6% used motor oil at 25°C has shown in Fig. 6. Four different models including power law, Bingham, Herschel-Buckley (H-B), and Hyperbolic models have been used. All the model parameters with their accuracy predictions have summarized in Table 3. The maximum measured shear stress for 6% bentonite drilling mud contaminated with 6% used motor oil at 25°C was 12.2 Pa at a shear strain rate of 1700 (1/s). Almost all the models predicted the maximum shear stress very well, and both the Bingham and hyperbolic models were the best with the highest R^2 of 0.95 and lowest RMSE of 0.48 Pa. The maximum shear stress for 6% bentonite drilling mud tested at 25°C increased by 42% as the used motor oil contamination increased from 0% to 6% because the used motor oil has lower density than clay particles that make the medium to have more clay particles in less volume leads to higher measured maximum shear stress.

Table 3. Models prediction parameters for 6% bentonite drilling mud contaminated with 6% used motor oil tested at 25°C

Bentonite (%)	Salt (%)	Oil (%)	Power law					Bingham			
			τ_0 (Pa)	K	n	RMSE (Pa)	R^2	τ_0 (Pa)	μ (cP)	RMSE (Pa)	R^2
6	0	6	4.86	0.94	0.32	1.12	0.78	4.42	0.0044	0.48	0.95	-

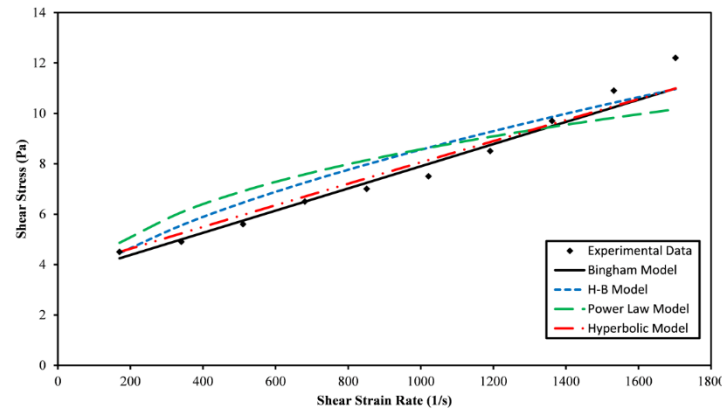| Bentonite (%)	Salt (%)	Oil (%)	Herschel- Buckley (H-B)					Hyperbolic				
			τ_0 (Pa)	k (Pa.s)	n	RMSE (Pa)	R^2	τ_0 (Pa)	A (Pa^{-1})	B $(Pa)^{-1}$	RMSE (Pa)	R^2
6	0	6	4.45	0.085	0.62	0.79	0.89	4.5	230	0.004	0.53	0.95

Figure 6. The variation of shear stress with shear strain rate for 6% bentonite drilling mud contaminated with 6% used motor oil tested at 25°C
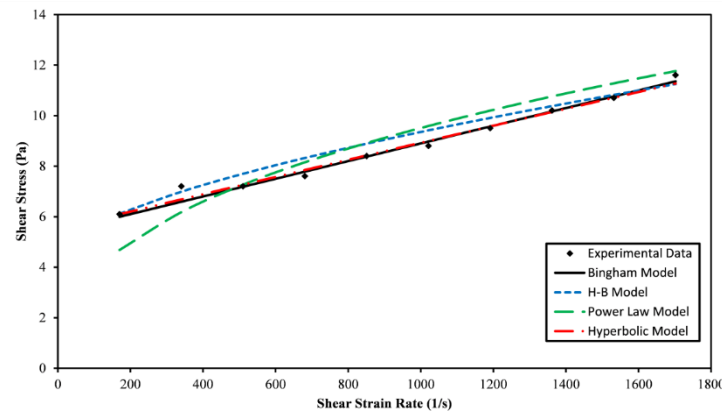

Figure 7. The variation of shear stress with shear strain rate for uncontaminated 6% bentonite drilling mud tested at 50° C

4.5. Experimental tests at 50°C

The variation of shear stress with a shear strain rate of uncontaminated 6% bentonite drilling mud at 50°C has shown in Fig. 8. Four different models including power law, Bingham, Herschel-Buckley (H-B), and Hyperbolic models have been used. All the model parameters with their accuracy predictions have summarized in Table 4. The maximum measured shear stress for uncontaminated 6% bentonite drilling mud at 50°C was 11.6 Pa at a shear strain rate of 1700 (1/s). All the models predicted the maximum shear stress very well with the highest R^2 of 0.98 and lowest RMSE of 0.22 Pa. The maximum shear stress for uncontaminated 6% bentonite drilling mud increased by 35% as the testing temperature increased from 25° C to 50°C.

Table 4. Models prediction parameters for uncontaminated 6% bentonite drilling mud tested at 50° C

			Power law					**Bingham**			
Bentonite (%)	Salt (%)	Oil (%)	τ_0 (Pa)	K	n	RMSE (Pa)	R^2	τ_0 (Pa)	μ (cP)	RMSE (Pa)	R^2
6	0	0	4.6	0.6	0.4	0.73	0.80	5.9	0.0035	0.22	0.98	-

			Herschel- Buckley (H-B)					**Hyperbolic**			
Bentonite (%)	Salt (%)	Oil (%)	τ_0 (Pa)	k (Pa.s)	n	RMSE (Pa)	R^2	τ_0 (Pa)	A (Pa^{-1})	B $(Pa)^{-1}$	RMSE (Pa)	R^2
6	0	0	6.11	0.067	0.62	0.42	0.93	6.1	290	0.004	0.22	0.98

The variation of shear stress with a shear strain rate of 6% bentonite drilling mud contaminated with 6% salt at 50°C has shown in Fig. 9. Four different models including power law,

Bingham, Herschel-Buckley (H-B), and Hyperbolic models have been used. All the model parameters with their accuracy predictions have summarized in Table 5. The maximum measured shear stress for 6% bentonite drilling mud contaminated with 6% salt at 50°C was 5.7 Pa at a shear strain rate of 1700 (1/s). All the models predicted the maximum shear stress very well, and the hyperbolic model was the best with the highest R^2 of 0.98 and lowest RMSE of 0.16 Pa. The maximum shear stress for 6% bentonite drilling mud tested at 50° C decreased by 104% as the salt contamination increased from 0% to 6%. The maximum shear stress for 6% bentonite drilling mud contaminated with 6% salt decreased by 2% as the testing temperature increased from 25°C to 50°C.
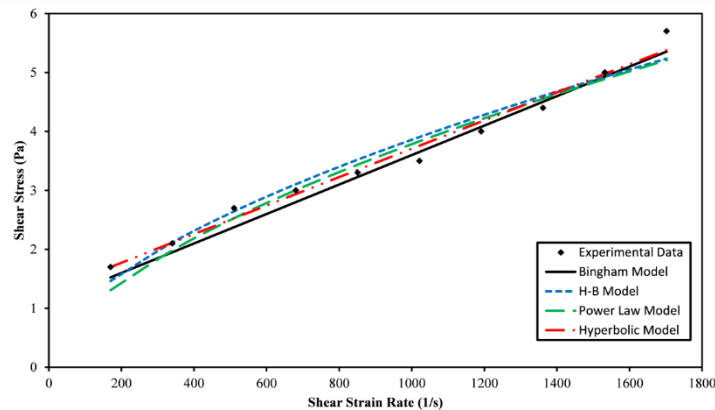

Figure 8. The variation of shear stress with shear strain rate for 6% bentonite drilling mud contaminated with 6% salt tested at 50°C
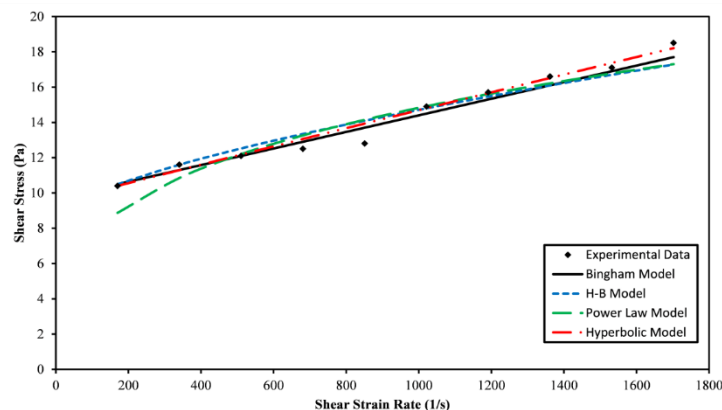

Figure 9. The variation of shear stress with shear strain rate for 6% bentonite drilling mud contaminated with 6% used motor oil tested at 50°C

Table 5. Models prediction parameters for 6% bentonite drilling mud contaminated with 6% salt tested at 50°C

Bentonite (%)	Salt (%)	Oil (%)	Power law					Bingham			
			τ_0 (Pa)	K	n	RMSE (Pa)	R^2	τ_0 (Pa)	μ (cP)	RMSE (Pa)	R^2
6	6	0	1.3	0.06	0.6	0.25	0.95	1.5	0.0025	0.19	0.97	-

Bentonite (%)	Salt (%)	Oil (%)	Herschel- Buckley (H-B)					Hyperbolic			
			τ_0 (Pa)	k (Pa.s)	n	RMSE (Pa)	R^2	τ_0 (Pa)	A (Pa^{-1})	B $(Pa)^{-1}$	RMSE (Pa)	R^2
6	6	0	1.4	0.058	0.6	0.24	0.95	1.7	410	0.004	0.16	0.98

The variation of shear stress with a shear strain rate of 6% bentonite drilling mud contaminated with 6% used motor oil at 50°C has shown in Fig. 9. Four different models including

power law, Bingham, Herschel-Buckley (H-B), and Hyperbolic models have been used. All the model parameters with their accuracy predictions have summarized in Table 6. The maximum measured shear stress for 6% bentonite drilling mud contaminated with 6% used motor oil at 50°C was 18.5 Pa at a shear strain rate of 1700 (1/s). All the models predicted the maximum shear stress very well, and the hyperbolic model was the best with the highest R^2 of 0.97 and lowest RMSE of 0.43 Pa. The maximum shear stress for 6% bentonite drilling mud tested at 50°C increased by 59% as the used motor oil contamination increased from 0% to 6%. The maximum shear stress for 6% bentonite drilling mud contaminated with 6% used motor oil increased by 52% as the testing temperature increased from 25°C to 50°C.

Table 6. Models prediction parameters for 6% bentonite drilling mud contaminated with 6% used motor oil tested at 50°C

Bentonite (%)	Salt (%)	Oil (%)	Power law					Bingham			
			τ_0 (Pa)	K	n	RMSE (Pa)	R^2	τ_0 (Pa)	μ (cP)	RMSE (Pa)	R^2
6	0	6	8.87	2	0.29	0.83	0.89	10.5	0.0047	0.48	0.96	-

Bentonite (%)	Salt (%)	Oil (%)	Herschel- Buckley (H-B)					Hyperbolic				
			τ_0 (Pa)	k (Pa.s)	n	RMSE (Pa)	R^2	τ_0 (Pa)	A (Pa^{-1})	B $(Pa)^{-1}$	RMSE (Pa)	R^2
6	0	6	10.9	0.064	0.66	0.67	0.93	10.4	190	0.004	0.43	0.97

5. Conclusions

Based on the experimental results and model predictions of this study, the following conclusions can be advanced:

1. For the fluid loss prediction, the API model prediction increased nonlinearly with time where no limit on the maximum fluid loss has been encountered whereas the kinetic hyperbolic model limited the maximum fluid loss to the quantity (V_o+N/B). In addition, the effect of applied pressure has been neglected in the API model, but the kinetic hyperbolic model has taken into account the effect of applied pressure.
2. For the uncontaminated 6% bentonite drilling mud, the maximum fluid loss is increased by 20% as the applied pressure increased from 25 psi to 90 psi.
3. For the 6% bentonite drilling mud contaminated with 6% salt, the maximum fluid loss is increased by 10% as the applied pressure increased from 25 psi to 90 psi.
4. For the applied pressure of 25 psi, the maximum fluid loss is increased by 244% as the salt contamination increased from 0% to 6%. For the applied pressure of 90 psi, the maximum fluid loss is increased by 216% as the salt contamination increased from 0% to 6%.
5. For the 6% bentonite drilling mud contaminated with 6% used motor oil, the maximum fluid loss is increased by 21% as the applied pressure increased from 25 psi to 90 psi.
6. For the applied pressure of 25 psi, the maximum fluid loss is increased by 31% as the used oil contamination increased from 0% to 6%. For the applied pressure of 90 psi, the maximum fluid loss is increased by 32% as the used oil contamination increased from 0% to 6%.
7. The maximum measured shear stresses for uncontaminated 6% bentonite drilling mud were 8.6 Pa and 11.6 Pa at 25°C and 50°C respectively. However, the maximum measured shear stresses for 6% bentonite drilling mud contaminated with 6% salt were almost the same represented by 5.8 Pa and 5.7 Pa at 25°C and 50°C respectively.
8. The maximum measured shear stresses for 6% bentonite drilling mud contaminated with 6% used motor oils were 12.2 Pa and 18.5 Pa at 25° C and 50° C respectively.
9. The maximum shear stresses for 6% bentonite drilling mud tested at 25° C increased by 48% and 42% as the salt and oil contaminations increased from 0% to 60% respectively. The maximum shear stresses for 6% bentonite drilling mud tested at 50° C increased by 104% and 59% as the salt and oil contaminations increased from 0% to 60% respectively.

10. All the used models to predict the maximum shear stress were very good and the hyperbolic model was the best with the highest R^2 of 0.98 and lowest RMSE of 0.14 Pa.

Acknowledgements

Symbols

τ	Shear stress	V_m	Volume of solids in mud
γ	Shear strain rate	A_o	Filter area
K_1	Fluid consistency unit	t	Time
n_1	Power law exponent	μ	Mud viscosity
Y_P	Yield point	h_{mc}	Thickness of the filter mud cake
P_V	Plastic viscosity	f_{sm}	Volume fraction of solids in the mud
τ_{o1}	Yield stress	f_{sc}	Volume fraction of solids in the cake
$\dot{\gamma}$	Shear strain rate	L and p	Arbitrary constants
K_2	Correction parameter	A_1	Fluid loss parameter
n_2	Flow behavior index	B_1	Arbitrary constant
τ_{max}	Maximum shear stress	α_o	Arbitrary constant
A and D	Model parameters	V_o	Initial value of drilling mud infiltration
V_f	Volume of fluid loss	RMSE	Root mean square error
v_o	Initial volume of fluid loss	R^2	Coefficient of determination
k	Drilling mud permeability	y_i	The actual value
k_o	Initial permeability of drilling mud	x_i	The calculated value from the model
ΔP	Applied pressure	$\bar{y}$	The mean of actual values;
f_{sc}	Volume fraction of solid in cake	$\bar{x}$	The mean of calculated values
f_{sm}	Volume fraction in mud	N_2	The number of data points
M	$\sqrt{\dfrac{2k\Delta P\left(\dfrac{f_{sc}}{f_{sm}}-1\right)}{\mu}}A_o$	N	$\sqrt{\dfrac{2*k_o*\alpha_o*\Delta P}{\mu(T)}}*A_o$

References

[1] Makhoukhi B. Design of experiments on sodic activation of bentonite for using as water-based drilling fluids. Pet Coal, 2016; 58 (3): 368-381.

[2] Sami NA. Effect of magnesium salt contamination on the behavior of drilling fluids. Egyptian Journal of Petroleum, 2016; 25: 453–458.

[3] Azim RA. Evaluation of production potential of fractured geothermal systems due to cold fluid circulation under poro-thermo elastic conditions. Pet Coal, 2017; 59(6): 975-990.

[4] Vipulanandan C, Raheem AM. Characterizing ultra-soft soils and anchor-soil interaction for deepwater applications. Proceedings of the Twenty-fifth International Ocean and Polar Engineering Conference, Kona, Big Island, Hawaii, USA, June 21-26, pp. 1048-1054.

[5] Shadravan A, Amani M. HPHT 101-what petroleum engineers and geoscientists should know about high pressure high temperature wells environment. Energy Science and Technology, 2012; 4(2): 36-60.

[6] Aremu MO, Arinkoola AO, Salam KK, Ogunmola EO. Potential of local pH control additives for corrosion inhibition in water base drilling fluids. Pet Coal, 2017; 59(5): 611-619.

[7] Shijun N, Bin F, Shibin L, Xiang S, Xuan Z, Bing L. Technical measures for improving compatibility of cement slurry with CO_2 contaminated drilling fluid: a case study. Nat Gas Ind, 2013; 33(9): 91-96.

[8] Avci E. Effect of Salinity on flow properties of Drilling Fluids: an experimental approach. Pet Coal, 2018; 60(2): 232-235.

[9] Ming L., Wei W., Youzhi Z., Xiaowei C., Bin D., Xiaoyang G. Impact of drilling fluid additives on performance of the cement slurry by single-factor. Chem Eng Oil Gas, 2014; 43(3): 297-301.

[10]   Amede VG, Alfazazi U. Optimal drilling fluid rheological considerations for avoiding stuck pipe and fluid loss under HT horizontal well condition: Gulf of Guinea as a scenario. Pet Coal, 2017; 59(5): 703-709.

[11]   Fakhreldin YE, Sharji H, Aghbari SA, Al-Rashdi S. Novel technique to determine cement contamination,.In: SPE/IADC Middle East Drilling Technology Conference and Exhibition, 24-26 October 2011, Muscat, Oman.

[12]   Youzhia Z, Chaoyia S, Kunquanc Y, Xiaoyangd G, Hualia Z, Taoa Y, Mingd L. (2015). Contamination effects of drilling fluid additives on cement slurry. Natural Gas Industry B, 2015; 2: 354-359.

[13]   Amani M, Al-Jubouri M, Shadravan A. Comparative study of using oil-based mud versus water-based mud in HPHT fields. Adv Pet Explor Dev, 2012; 4: 18–27.

[14]   Nagre RD, Lin Zhao, Owusu PA. Thermosaline resistant acrylamide-based polyelectrolyte as filtration control additive in aqueous-based mud. Pet. Coal, 2014; 56(3): 222–230.

[15]   Darley HCH, Gray GR. Composition and properties of drilling and completion Fluids. Fifth ed., Gulf Professional Publishing 1988, Houston, Texas, USA.

[16]   Nasser J, Jesil A, Mohiuddin T, Al Ruqeshi M, Devi G, Mohataram S. Experimental investigation of drilling fluid performance as nanoparticles. World Journal of Nano Science and Engineering, 2013; 3: 57-61.

[17]   Ali K, Vipulanandan C, Richardson D. Salt (NaCl) contamination on the resistivity and plastic viscosity of a bentonite drilling mud. Proceedings of CIGMAT Conference & Exhibition 2013.

[18]   Basirat B, Vipulanandan C, Richardson D. Filtration loss in 4% bentonite drilling mud with xanthan gum. Proceedings of THC-IT Conference & Exhibition 2013.

[19]   Hassiba KJ, Amani M. The effect of salinity on the rheological properties of water based mud under high temperatures for drilling offshores and deep wells. Earth Sci. Res. J., 2013; 2(1): 175–186.

[20]   Adekomaya OA, Anifowose DM, Wale T. Experimental study of the effect of temperature on the flow properties of normal oil based muds in Niger delta formation. Pet. Coal, 2011; 53(2): 140–145.

[21]   Wang F, Tan X, Wang R, Sun M, Wang L, Liu J. High temperature and high pressure rheological properties of high-density water-based drilling fluids for deep wells. Pet. Sci., 2012; 9: 354–362.

[22]   Alaskari MKG, Teymoori RN. Effects of salinity, pH and temperature on CMC polymer and XC polymer performance. IJE Tran. B: Appl., 2007; 20(3): 283-290.

[23]   Studds PG, Stewart DI, Cousens TW. (1998). The effects of salt solutions on the properties of bentonite-sand mixtures. Clay Minerals, 1998; 33: 651-660.

[24]   Tang H, Kalyon D. Estimation of the parameters of Herschel–Bulkley fluid under wall slip using a combination of capillary and squeeze flow viscometers. Rheol. Acta, 2004; 43: 80–88.

[25]   Bourgoyne AT, Millheim KK, Chenevert ME, Young FS. Applied drilling engineering. SPE Foundation 1991, pp. 508.

[26]   Andrea SV, Hau G, Gerard DB, Pavel B, Pacelli LJ. A CT scan aided core-flood study of the leak-off process in oil-based drilling fluids. SPE International Symposium and Exhibition 2012, Louisiana, USA, pp.1-25.

[27]   Vipulanandan C, Raheem AM, Basirat B, Mohammed A, Richardson D. New kinetic model to characterize the filter cake formation and fluid loss in HPHT process. OTC, 25100-MS, Houston, TX, 5-8 May 2014, pp. 1-17.

[28]   Steel RGD, Torrie JH. Principles and procedures of statistics with special reference to the biological sciences. McGraw Hill 1960.

To whom correspondence should be addressed: Dr. Aram Mohammed Raheem, University of Kirkuk, Civil Engineering Department, Kirkuk, Iraq